Supporting Information

Versatile oxalato-bridging modes: a novel three-dimensional framework structure of manganese(II) oxalate complex $[MnC_2O_4]\cdot 0.5H_2O$ and the relationship with other manganese(II) oxalates

Wen-Yuan Wu,* Tie-Huan Tang, Yi Li and Shuang Xu

College of Chemistry and Molecular Engineering, Nanjing Tech University, Nanjing 211800, China

* Corresponding e-mail: wwy@njtech.edu.cn

Contents

1. Materials and instrumental

Unless otherwise specified, all starting materials were purchased from commercial sources and used as supplied. Manipulations were performed under normal atmospheric conditions unless otherwise noted. Thermo gravimetric analyses (TGA) and differential thermal analyses (DTA) were performed on a SDT thermal analyzer under a flowing atmosphere or nitrogen atmosphere with the rate of 100-150 mL / min. The heating temperature ranges from room temperature to 600 °C at the heating rate of 10 °C/min. The XRD analysis was carried out with a Simens powder diffractometer using Cu *K*α radiation (λ = 1.54056 Å). The 2θ ranges are set within 5-80 ° with a step of 0.02 °. The identification of the phases was realized by comparing the experimental XRD powder patterns to the JCPDS standard data. For single XRD measurement, data were collected at room temperature on a Bruker Smart APEX CCD diffractometer, using graphite monochromated Mo-Kα radiation (λ=0.71073Å). Magnetic susceptibilities χ were measured on a SQUID magnetometer (Quantum Design, MPMS) between 1.8 and 300 K in an applied field of 2000 Oe. Specific heat Cp was recorded between 2 and 30 K by a pulse relaxation method using a commercial calorimeter (Quantum Design PPMS).

2. Synthesis of complex $[MnC_2O_4]\cdot 0.5H_2O$ (1).

A mixture of $Mn(OAc)\cdot 4H_2O$ (0.2451g, 1 mmol), malonic acid (0.2081g, 2 mmol), $H_2C_2O_4\cdot 2H_2O$ (0.1261g, 1 mmol) and distilled water (15 mL) was heated at the temperature of 150℃ for 3 days in a 23 mL Teflon-lined autoclave. The starting pH value of the solution was 2, while the final pH was 4 after the hydrothermal treatment. After being washed by distilled water and then anhydrous acetone, the insoluble pink crystals were collected by filtration and then dried in the air. The final product (Yield 90.0 mg, 59 %) was proved to be single phase by the judgments of element analysis and X-ray powder diffraction determination (Found: C, 15.95 wt%; H 0.60 wt%. Calcd: C 15.81 wt%; H 0.66 wt%). IR (KBr pellet, cm^{-1}): 3418(board), 1638(strong), 1320(strong), 790(strong), 518(moderate).

3. Crystallography for 1

Crystals of **1** with the shape of hexangular plate were manually picked out for single crystal structural determination. Data were collected at room temperature on a Bruker Smart APEX CCD diffractometer, using graphite monochromated Mo-Kα radiation (λ=0.71073Å). Empirical correction based on symmetry equivalent reflections was applied to collected data by using the SADABS program. 2019 reflections were collected with 454 data unique. Structure was solved by direct method and refined by least-squares method on F^2. All non-hydrogen atoms were refined anisotropically. Hydrogen atoms in water molecules were placed in calculated positions and refined as riding atoms. Final R values: R_1=0.0359 for all data and wR_2=0.0981 for 416 reflections with I>2σ. CCDC-2024513 contains full supplementary crystallographic data.

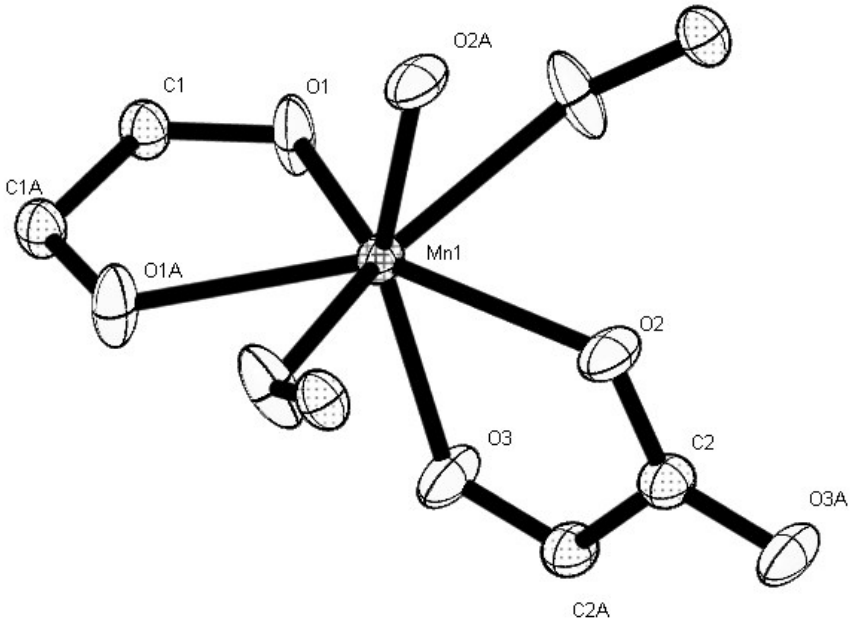

Figure S1. The coordination environment of Mn atom in **1**, showing the unusual seven-coordinated mode. Thermal ellipsoids are set at 50% probability. C2, C2A, O2, O2A, O3 and O3A are from interlayer oxalates, while others are from layer structure.

Table S1. Hydrogen bond lengths (Å) and angle (°) for $[MnC_2O_4]\cdot 0.5H_2O$ (**1**)

D-H…A	D-H	H…A	D…A	< D-H…A
O4-H1…O1	0.85	2.30	3.134(3)	167

4. Powder X-ray diffraction study of manganese(II) oxalates 1 & 2

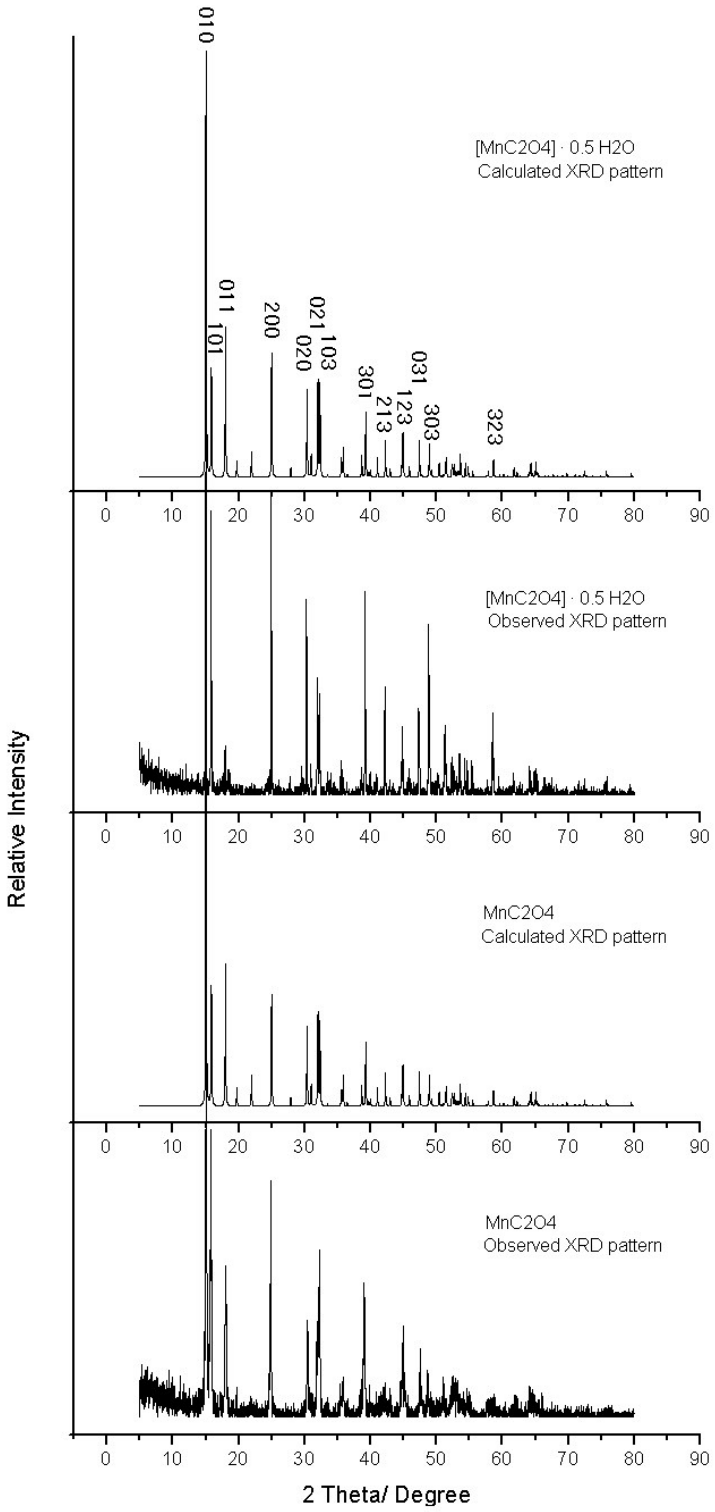

Figure S2. Calculated and observed XRD powder patterns for $[MnC_2O_4]\cdot 0.5H_2O$ (**1**) and α-MnC_2O_4 (**2**).

5. Thermal behaviors of manganese(II) oxalates 1 & 2

5.1 $[MnC_2O_4]\cdot 0.5H_2O$ (**1**)

Under the atmosphere of flowing air (Figure S3a), the dehydration of **1** started at 110 ºC and continued until 140 ºC, with endothermal peak at 130 ºC. The total weight loss at 200 ºC was 6.08 %, which meets the theoretical one of 5.92 %. The second stage of weight loss caused by decomposition and oxidation started at 220 ºC and did not end until 480 ºC. There were two exothermal peaks during the second stage. The main peak occurred at 391 ºC, while the much smaller peak at 319 ºC. The final weight loss at 500 ºC was 57.40 %, which is close to the calculated value of an expected product for MnO (53.32 %).

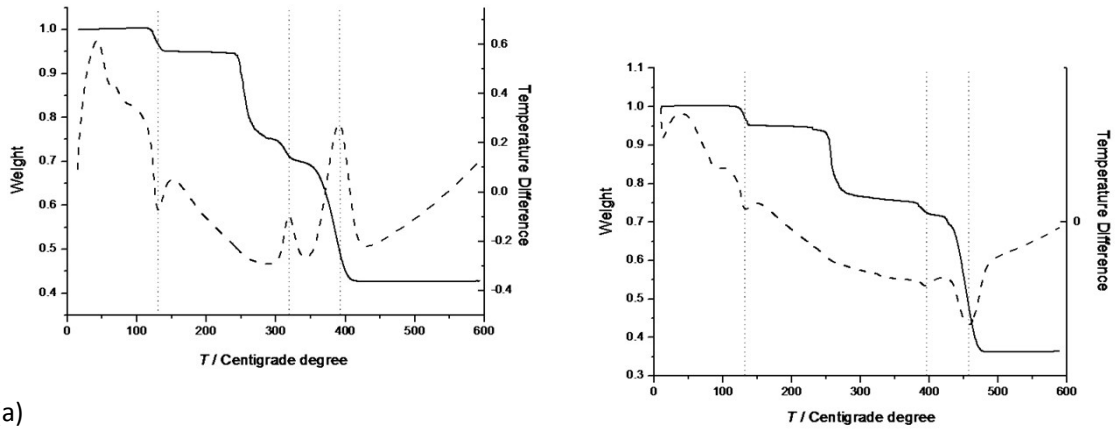

(a)

（b）

Figure S3. (a) TGA (solid line) and DTA (dash line) curves for **1** under the atmosphere of air; (b) under the atmosphere of nitrogen.

Under the atmosphere of flowing nitrogen (Figure S3b), the dehydration of **1** started at 115 ºC and continued until 135 ºC, with endothermal peak at 131 ºC. The total weight loss at 200 ºC was 6.03 %, which meets the theoretical one of 5.92 %. The second stage of weight loss caused by decomposition started at 220 ºC and did not end until 480 ºC. There were two endothermal peaks during the second stage. The main peak occurred at 457 ºC, while the much smaller peak at 395 ºC. The final weight loss at 500 ºC was 63.84 %, which is identical with the calculated value of an expected product for metal Mn (63.85 %).

There is no obvious difference in the dehydration stage between the two atmospheres. However the endothermal peaks under the atmosphere of nitrogen occur

at higher temperatures than the exothermal peaks under the atmosphere of air, where an oxidation course is obviously involved.

5.2 α-MnC_2O_4 (**2**)

Under the atmosphere of flowing air (Figure S4a), the total weight loss for **2** at 200 ºC was 1.51 %, which shows the slight water adsorption of the sample. The decomposition and oxidation stage started at 265 ºC and did not end until 345 ºC, where is an exothermal peaks at 310 ºC. Also there is another much smaller exothermal peak at 460 ºC, which results minor weights lose (about 1 % in total weight). The final weight loss at 500 ºC was 48.28 %, which is between the calculated values of an expected product for Mn_3O_4 (46.65 %) and for MnO (50.38 %).

Under the atmosphere of flowing nitrogen (Figure S4b), the total weight loss for **2** at 200 ºC was 1.66 %, which also shows the slight water adsorption of the sample. The decomposition stage starts at 320 ºC and did not end until 435 ºC. There is an endothermal peak at 412 ºC. The final weight loss at 500 ºC was 49.89 %, which is close to the calculated value of an expected product for MnO (50.38 %).

α-MnC_2O_4 seems to be more stable in the nitrogen than in the air. In the latter situation, it begins to decompose at the temperature of 320 ºC and absorbs heat from environment, while in the former it starts to decompose at 265 ºC and releases heat to environment where an oxidation course is obviously involved.

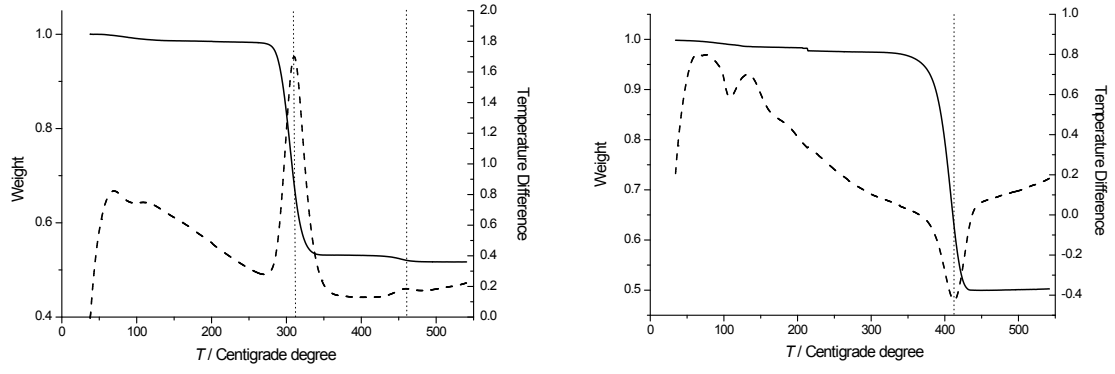

(a) (b)

Figure S4. (a) TGA (solid line) and DTA (dash line) curves for **2** under the atmosphere of air; (b) under the atmosphere of nitrogen.

Table S2. Calculated weight loss (%) of the manganese(II) oxalates **1** & **2**

Compound (FW)	Mn_2O_3 (157.87)	Mn_3O_4 (228.81)	MnO (70.94)	Mn (54.94)
1 (142.96)	44.79	46.65	50.38	61.57
2 (151.97)	48.06	49.81	53.32	63.85

5.3 Isothermal annealing of manganese(II) oxalates **1**

According to the TGA and DTA results, the decomposition occurs in the temperature range between 220 and 480 ºC. So the isothermal temperature is set at 500 ºC, when the sample of **1** was annealed in the air for 1 hour. The final product was determined on the basis of the X-ray powder patterns (JCPDS 24-0734 for Mn_3O_4 and JCPDS 41-1442 for α-Mn_2O_3).

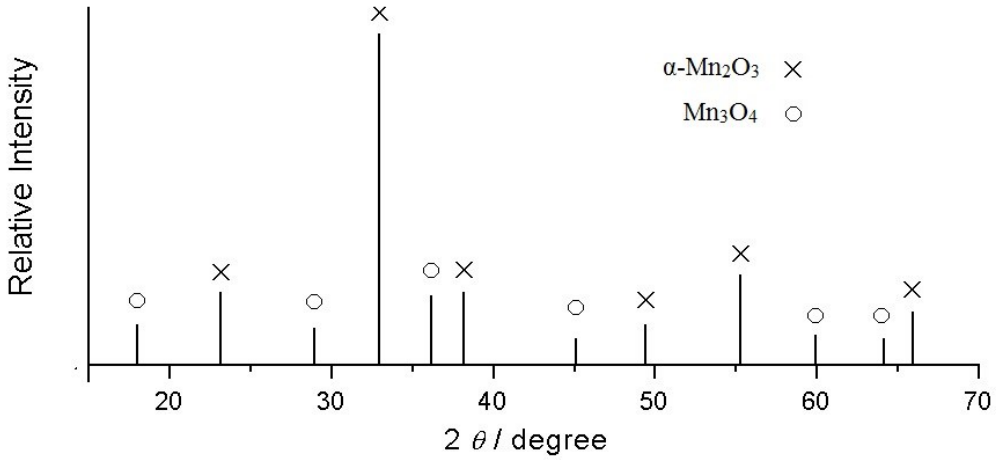

Figure S5. The X-ray powder pattern showing the phase composition of the thermal annealing product for **1**.

6. Magnetic behaviors of manganese(II) oxalates 1 & 2

6.1 $[MnC_2O_4]\cdot 0.5H_2O$ (**1**)

Variable-temperature magnetic susceptibility of **1** was measured on powdered sample from 300 to 1.8 K, showing the typical antiferromagnetic interaction between Mn^{II} ions (Figure S6). The χ_M value increases continuously upon cooling, reaching the sharp maximum of 0.0823 $cm^3\ mol^{-1}$ around 14 K, then decreases to 0.0662 $cm^3\ mol^{-1}$ at 1.8 K. The $\chi_M T$ value drops all along the cooling course and the effective magnetic moment per Mn^{II} ion, 5.83 μ_B, calculated from $\chi_M T$ value at 300 K is somewhat

smaller than the spin-only value (5.92 μ_B) expected for a high spin configuration (S = 5/2), which also shows the existence of antiferromagnetic coupling. The magnetic susceptibility of **1** above 30 K is fitted well with the Curie-Weiss law, giving the parameters of C = 4.75 cm^3 K mol^{-1} and θ = -34.77 K. Néel temperature is determined by the specific heat measurement that exhibits a sharp peak at 11.2(1) K (Figure S7).

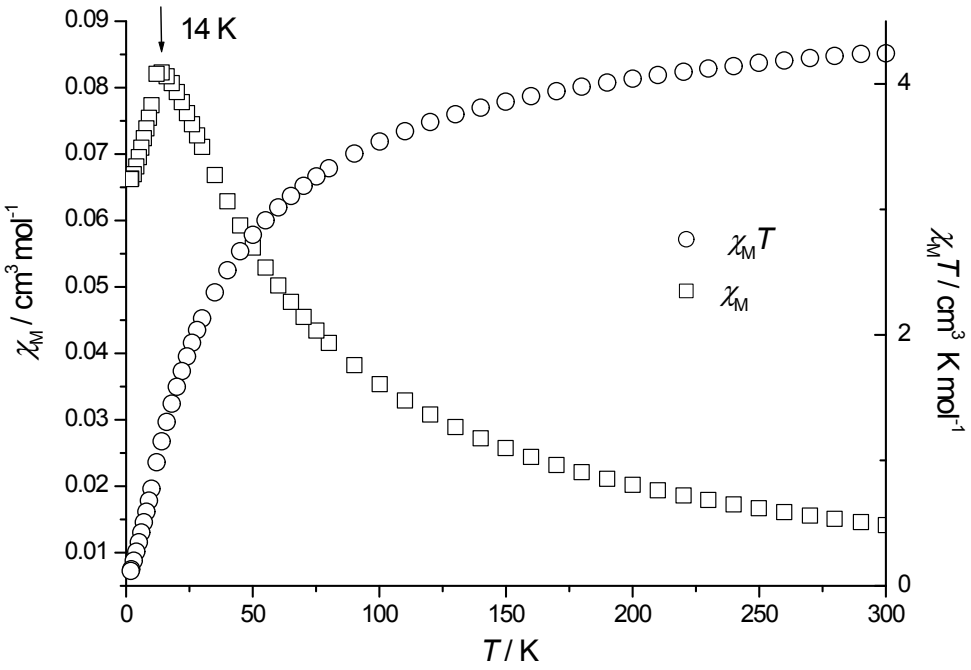

Figure S6. Thermal variations of $\chi_M T$ and χ_M for **1**.

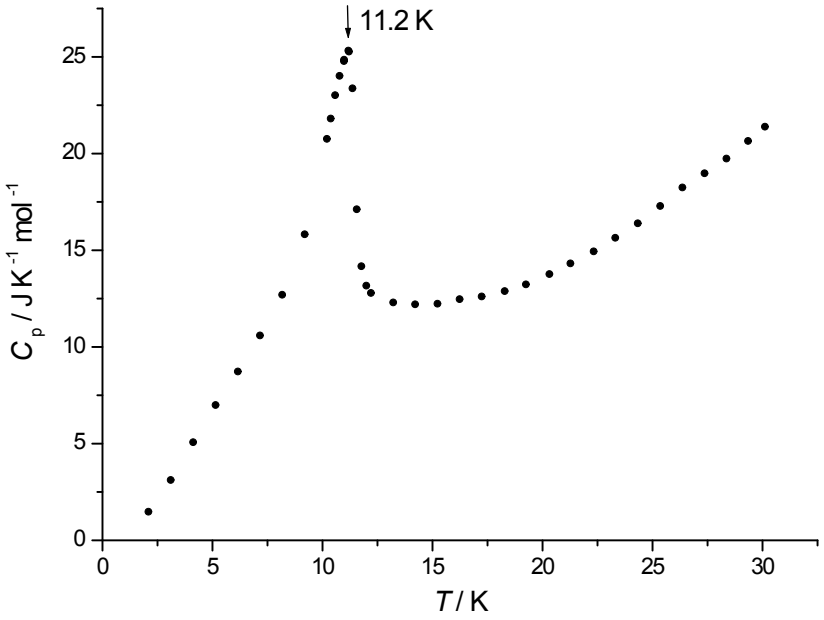

Figure S7. Specific heat C_p plotted against temperature shows a peak at T_N = 11.2(1) K for **1**

6.2 α-MnC_2O_4 (**2**)

Variable-temperature magnetic susceptibility of **2** was measured on powdered sample from 300 to 1.8 K, showing the typical antiferromagnetic interaction between Mn^{II} ions (Figure S8). The χ_M value increases continuously upon cooling, reaching the sharp maximum of 0.0756 cm^3 mol^{-1} around 14 K, then decreases to 0.0630 cm^3 mol^{-1} at 1.8 K. The $\chi_M T$ value drops all along the cooling course and the effective magnetic moment per Mn^{II} ion, 5.61 μ_B, calculated from $\chi_M T$ value at 300 K is somewhat smaller than the spin-only value (5.92 μ_B) expected for a high spin configuration (S = 5/2), which also shows the existence of antiferromagnetic coupling. The magnetic

susceptibility of **2** above 30 K is fitted well with the Curie-Weiss law, giving the parameters of C = 4.38 cm^3 K mol^{-1} and θ = -32.27 K. Néel temperature is determined by the specific heat measurement that exhibits a sharp peak at 9.9(2) K (Figure S9).

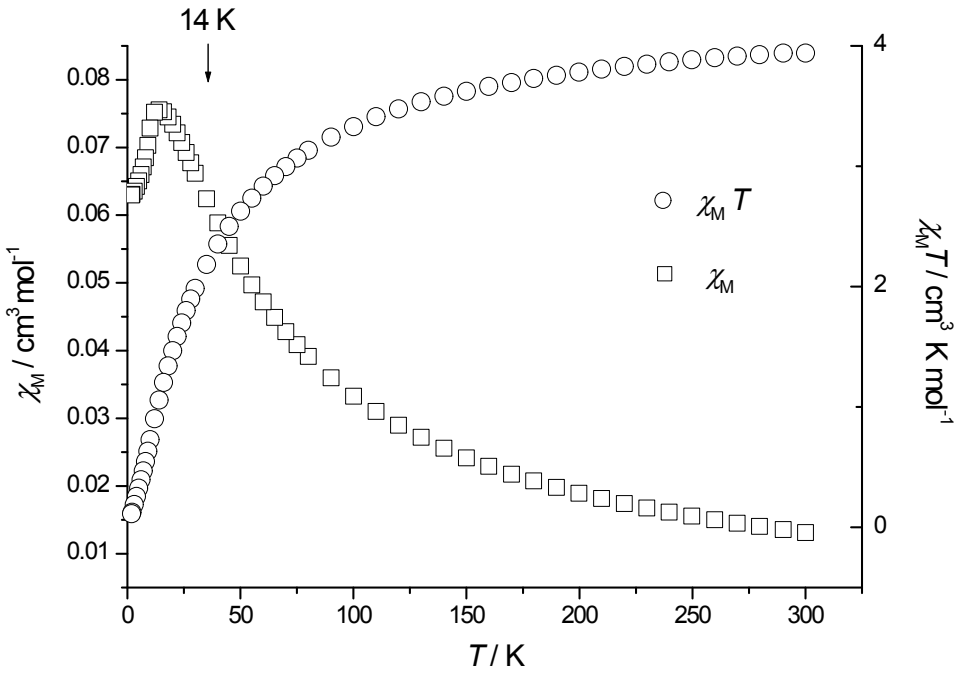

Figure S8. Thermal variations of $\chi_M T$ and χ_M for **2**.

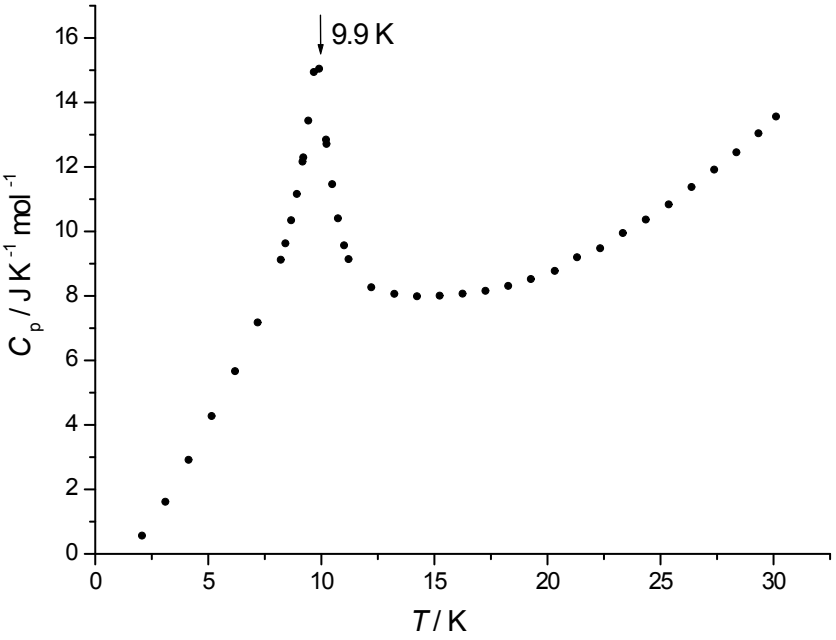

Figure S9. Specific heat C_p plotted against temperature shows a peak at T_N = 9.9(2) K for **2**.